The Astrophysical Journal, 857:123 (5pp), 2018 April 20 https://doi.org/10.3847/1538-4357/aab848

The X-Ray Modulation of PSR J2032+4127/MT91 213 during the Periastron Passage in 2017

K. L. Li[1], J. Takata[2], C. W. Ng[3], A. K. H. Kong[4], P. H. T. Tam[5], C. Y. Hui[6], and K. S. Cheng[3]
[1] Department of Physics and Astronomy, Michigan State University, East Lansing, MI 48824, USA; liliray hk@gmail.com
[2] School of Physics, Huazhong University of Science and Technology, Wuhan 430074, People's Republic of China
[3] Department of Physics, The University of Hong Kong, Pokfulam Road, Hong Kong
[4] Institute of Astronomy, National Tsing Hua University, Hsinchu 30013, Taiwan
[5] School of Physics and Astronomy, Sun Yat-sen University, Zhuhai 519082, People's Republic of China
[6] Department of Astronomy and Space Science, Chungnam National University, Daejeon 305-764, Republic of Korea
Received 2018 February 9; revised 2018 March 3; accepted 2018 March 18; published 2018 April 24

Abstract

We present the *Neil Gehrels Swift Observatory* (*Swift*), *Fermi Large Area Telescope* (*Fermi*-LAT), and *Karl G. Jansky Very Large Array* (VLA) observations of the γ-ray binary PSR J2032+4127/MT91 213, of which the periastron passage recently occurred in 2017 November. In the *Swift* X-ray light curve, the flux was steadily increasing before 2017 mid-October, however, a sharp X-ray dip on a weekly timescale is seen during the periastron passage, followed by a post-periastron X-ray flare lasting for ~20 days. We suggest that the X-ray dip is caused by (i) an increase of the magnetization parameter at the shock, and (ii) the suppression due to the Doppler boosting effect. The 20-day post-periastron flare could be a consequence of the Be stellar disk passage by the pulsar. An orbital GeV modulation is also expected in our model; however, no significant variability is seen in the *Fermi*-LAT light curve. We suspect that the GeV emission from the interaction between the binary's members is hidden behind the bright magnetospheric emission of the pulsar. The pulsar gating technique would be useful to remove the magnetospheric emission and recover the predicted GeV modulation, if an accurate radio timing solution over the periastron passage is provided in the future.

Key words: pulsars: individual (PSR J2032+4127) – stars: individual (MT91 213) – stars: winds, outflows – X-rays: binaries

1. Introduction

PSR J2032+4127 is a young pulsar that has shown pulsations at a spin period of $P_s = 143.2$ ms in both γ-rays (Abdo et al. 2009) and radio (Camilo et al. 2009; Ray et al. 2011). A subsequent timing study by Lyne et al. (2015) indicated that PSR J2032+4127 is orbiting in a highly eccentric orbit with the Be star MT91 213 in the Cyg OB2 stellar association (Massey & Thompson 1991). Based on the latest timing solution published by the team, the binary has a very long orbital period of 45–50 years with an eccentricity of $e = 0.94$–0.99, and the pulsar would have reached periastron in 2017 November (Ho et al. 2017).

The binary PSR J2032+4127/MT91 213 (hereafter J2032) has been suggested to be a γ-ray binary: a subclass of high-mass X-ray binaries (HMXBs) with members that show high-energy (HE; 0.1–100 GeV) and/or very-high-energy (VHE; >100 GeV) orbital modulations in their highly eccentric orbits (see, e.g., Dubus 2013). While the pulsed emission of J2032 could be too bright to dominate over the possible HE modulation in GeV (Takata et al. 2017), VERITAS and MAGIC found that the TeV emission of J2032 increased by a factor of ~10 from 2017 June/August to November (Mirzoyan & Mukherjee 2017; VERITAS & MAGIC Collaborations 2017). In addition to VHE, the X-ray emission of J2032 has been rapidly increasing in 2016–17 (Ho et al. 2017; Li et al. 2017), and this pre-periastron X-ray enhancement is commonly seen in other γ-ray binaries, e.g., PSR B1259−63/LS 2883 (Chernyakova et al. 2015; Tam et al. 2015). Takata et al. (2017) proposed an intra-binary shock model, which involves an evolving pulsar wind magnetization and the Doppler Boosting effect, to explain the pre-periastron X-ray rise. Alternatively, Petropoulou et al. (2018) adopted an axisymmetric (no azimuthal dependence) stellar wind structure to explain the observed X-ray light curve. Aside from the global increasing trend, Li et al. (2017) found strong spectral variability on a monthly timescale in X-rays, but the mechanism behind it still remains unclear.

In this paper, we report the new *Swift* observations taken during the periastron passage. *Fermi*-LAT observations are also presented, however, no significant γ-ray variability can be detected. We also discussed how such an X-ray modulation can be formed with the pulsar wind/stellar wind interaction model (Takata et al. 2017). Throughout the analysis, we assumed the periastron date to be 2017 November 12 (MJD 58069) as suggested by the `Model 2` in Ho et al. (2017), although 2017 November 13 as the the periastron date was derived in some recent *Astronomer*'s *Telegrams* (e.g., Coe et al. 2017).

2. *Swift* Observations

Swift has been intensively monitoring J2032 since early 2016, with a weekly cadence before mid-2017 to a daily cadence around periastron in 2017 November. As of 2018 January 31, 177 usable observations can be found in the *Swift* public data archive (six of them were taken before 2016). Most of them have exposure times between 1 and 4 ks, and a few have 5 ks or more.

2.1. XRT Data Reduction

The *Swift*/X-Ray Telescope (XRT) online tools[7] (`HEAsoft` v6.22 based) are used to build the light curve and the spectra

[7] http://www.swift.ac.uk/user_objects/index.php

used in this study (Evans et al. 2007, 2009). Except for switching (i) the binning method to `Observation`, (ii) the centroid method to `Iterative`, and (iii) the minimum significance for a detection to two, all default parameters were adopted. In addition, we manually subtracted the expected contribution from the three XRT-unresolved sources (i.e., 1.7×10^{-3} cts s^{-1}) in the light curve to avoid an overestimation of the X-ray emission (see the detailed calculation in Li et al. 2017). To compute the count rate to flux conversion factor, we extracted spectra using the observations from 2017 April 06 to 2017 November 12 (arbitrarily chosen) and fitted them with an absorbed power law simultaneously (all of the parameters are tiled except the normalizations). The best-fit parameters are $N_{\rm H} = 1.1 \times 10^{22}$ cm^{-2} and $\Gamma = 1.6$, which yield a conversion factor of 1.142×10^{-10} erg cm^{-2} cts^{-1} (for unabsorbed flux in 0.3–10 keV). We also tried some other combinations of spectra and the conversion factor does not change significantly. Finally, although the XRT data qualities do not allow a good time-resolved spectral analysis over the periastron passage, we calculated the hardness ratio for each epoch to study the evolution of the X-ray color (i.e., H/S, where S is the soft X-ray count rate in 0.3–1.5 keV and H is the hard X-ray count rate in 1.5–10 keV; Figure 2).

2.2. UVOT Data Reduction

`HEAsoft` (v6.22) with the UVOT `CALDB` (v201709221) was used to reduce the UVOT observations. All six UVOT filters have been used (one filter per observation in most of the cases), however, the *v*- and *b*-band light curves are undersampled and are therefore not discussed in this paper.

The *Swift*-specific `FTOOLS`, `uvotmaghist`, was used to extract the UV light curves using aperture photometry. The source aperture was chosen to be a 3″ radius circular region, which is the optimal size for the UVOT data.[8] Two bright sources are fairly close to J2032. To accurately account for the contamination from them, we used a 3″ circular region as the background region, at a position so that the distances from the two nearby sources are the same as the distances between the nearby sources and J2032. Although the *u*-band images are slightly overexposed as MT91 213 is very bright with $m_v = 11.95$ mag (Reed 2003), the flags `saturated=0` from `uvotmaghist` suggest that the measurements are still usable.

3. *Fermi*-LAT Observations

To obtain the γ-ray long-term light curve of J2032, we downloaded the *Fermi* "Pass 8 Source" LAT data (instrumental response function: "P8R2_SOURCE_V6") from the *Fermi* Science Support Center (FSSC)[9] with the criteria of (i) energy from 100 MeV to 500 GeV, and (ii) time from 2008 August 04 to 2018 January 22. A region of interest (ROI) was chosen to be 20° × 20° square centered at the epoch J2000 position of the source: (R.A., decl.) = ($20^{\rm h}32^{\rm m}14\overset{\rm s}{.}35$,+41°26′48″.8; i.e., the LAT position of J2032 in the *Fermi* LAT 4-Year Point Source Catalog (3FGL); Acero et al. 2015). In addition, all of data observed at zenith angles greater than 90° were excluded to avoid contamination from the Earth's albedo. All of the data reduction and analysis processes were performed using the *Fermi* Science Tools package version v10r0p5.

We first used the `gtlike` tool to model the average emission from the background sources between 2008 August 04 to 2017 October 19 with a maximum likelihood optimization technique (i.e., the binned likelihood analysis). The source model includes (i) all of the 3FGL cataloged sources within 25° from the center of the ROI (gll_psc_v16.fit; Acero et al. 2015); (ii) the galactic diffuse emission (gll_iem_v06), and the isotropic diffuse emission (iso_P8R2_SOURCE_V6_v06); and (iii) the nearby microquasar Cygnus X-3 (Bodaghee et al. 2013) located $<0\overset{\circ}{.}5$ away from J2032 (a simple power-law spectral model was assumed). For those 3FGL sources that are non-variable and located >6° away from the ROI center, all of the spectral parameters were fixed to their listed values in the 3FGL. There are also four extended sources in the source model: Gamma Cygni, Cygnus Cocoon, HB 21, and Cygnus Loop, which were modeled by the extended source templates obtained from the FSSC. Our target J2032, known as 3FGL J2032.2+4126 in the 3FGL catalog, was described by a power law with simple exponential cutoff in the source model,

$$\frac{{\rm d}N}{{\rm d}E} = N_0\left(\frac{E}{E_0}\right)^{-\Gamma}\exp\left(-\frac{E}{E_C}\right), \quad (1)$$

where N_0 is the normalization constant, E_0 is the scale factor of energy in MeV, Γ is the spectral power-law index, and E_C is the cutoff energy in MeV. From the binned likelihood analysis, the best-fit parameters of J2032 during 2008 August 04 to 2017 October 19 are $N_0 = (1.66 \pm 0.05) \times 10^{-11}$, $\Gamma = -1.39 \pm 0.04$, and $E_C = (4500 \pm 249)$ MeV.

Next, we construct a new model from the above version by fixing all of the spectral parameters to their global best-fit values, except the normalizations. The new model was then used to compute a long-term two-week binned light curve of J2032 with the binned likelihood method, which is shown in Figure 1. In addition, the light curve of Cyg X-3 is shown for comparison. As shown in the bottom panel of the figure, Cyg X-3 was mostly undetected at $\sim 3\sigma$ significance level around the periastron passage, indicating that the observed variability of J2032, however weak, is unlikely to be related to the transient nature of Cyg X-3. It is also important to note that the light curve shows the total energy fluxes observed at the position of J2032, which is the sum of the pulsar's magnetospheric emission (which is the dominant component) and the possible contribution from the interaction between the binary's members.

4. Very Large Array (VLA) Observation

We observed J2032 with the VLA at 3 GHz (2–4 GHz; S-band) in the C configuration on 2017 August 14, from 05:10:40 to 05:43:20 UTC (the observing date was marked in Figure 2), under a Director Discretionary Time (DDT). Standard data reduction procedures were performed using the CASA software package (v4.7.2). J2032 was clearly detected with an average flux of $S_3 = 0.10$ mJy beam^{-1} (background rms noise: 0.014 mJy beam^{-1}). The obtained flux is well consistent with the previous measurement taken in 2009 (i.e., $S_2 = 0.12$ mJy at 2 GHz; Camilo et al. 2009), implying that the system did not evolve much at least in August (three months before the periastron passage). It is worth noting that the VLA observation was taken near the first peak of the X-ray light curve (Figure 2). While the X-rays

[8] https://swift.gsfc.nasa.gov/analysis/threads/uvot_thread_aperture.html
[9] http://fermi.gsfc.nasa.gov/ssc/

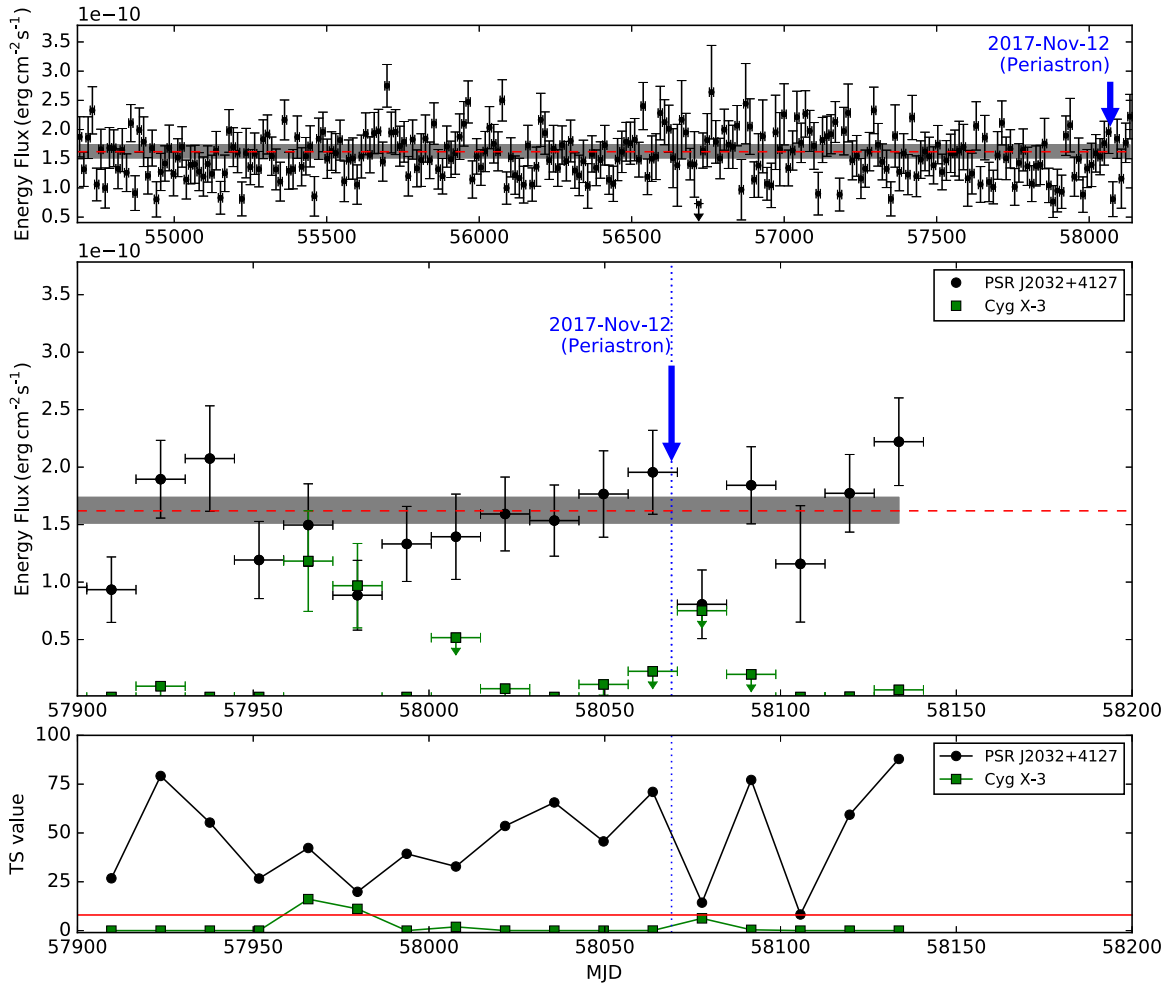

Figure 1. Top panel: *Fermi* γ-ray light curve of J2032 during 2008 August 04 to 2018 January 22 in the energy range 100 MeV–500 GeV. Middle panel: zoom-in version of the light curve showing the energy flux of J2032 (circle) and the nearby Cyg X-3 (square) from 2017 May 27 to 2018 January 22. In both light curves, the blue arrow shows the time of the periastron passage, while the red dashed line represents the average flux level of the source from the global binned likelihood analysis during 2008 August 04 to 2017 October 19 with the corresponding uncertainty indicated by the gray shaded band. Bottom panel: test-statistic (TS) values of J2032 and Cyg X-3. The red solid line indicates the TS threshold of 8, under which an 95% upper limit (triangle) is determined in the above light curves.

increased by a factor of 4 from 2016 to 2017, the radio remains roughly the same.

5. Discussions

5.1. X-Ray Modulation

The observed X-ray flux of J2032 showed a rapid increase in 2013–2016, and then it abruptly began to decrease in 2017 October just before the periastron passage in early November. In addition, the X-ray hardness ratio likely increased (i.e., harder) when the pulsar was passing periastron, possibly because of the higher $N_{\rm H}$, hence the heavier soft X-ray absorption, near the Be star. Despite the small-scale fluctuation and/or flare-like behaviors observed soon after the periastron passage that could be related to the interactions between the pulsar and the clumpy stellar wind and/or the Be stellar disk, the global trend of the observed X-ray light curve can be explained by the evolution of the magnetization of the pulsar wind and the Doppler boosting effect of the shocked pulsar wind. The magnetization of the pulsar wind is defined by the ratio of the magnetic energy to the kinetic energy

$$\sigma = \frac{B^2}{4\pi\Gamma_{\rm PW} N_{\rm PW}\, m_e c^2}, \quad (2)$$

where B, $\Gamma_{\rm PW}$, and $N_{\rm PW}$ are the magnetic field, Lonrentz factor, and number density of the cold-relativistic pulsar wind, respectively, at the region between the pulsar and the shock. It has been a long-standing problem of how the magnetization evolves with distance from $\sigma \gg 1$ at the light cylinder to $\sigma < 1$ at the interstellar shock of the pulsar wind nebula (see, e.g., Kennel & Coroniti 1984; Coroniti 1990; Lyubarsky & Kirk 2001). Kirk & Mochol (2011) and Kirk & Giacinti (2017) suggested that the evolution can be described by $\sigma \propto r^{-1}$ (here r means the radial distance from the pulsar) for the regions far away from the light cylinder in the absence of the magnetic dissipation. The evolution can be steeper if there is a magnetic dissipation in the pulsar wind.

We have modeled the X-ray modulation of J2032 over the periastron passage by assuming a radial dependency of the magnetization as $\sigma \propto r^{-\alpha}$, where α is in the range of 1–3

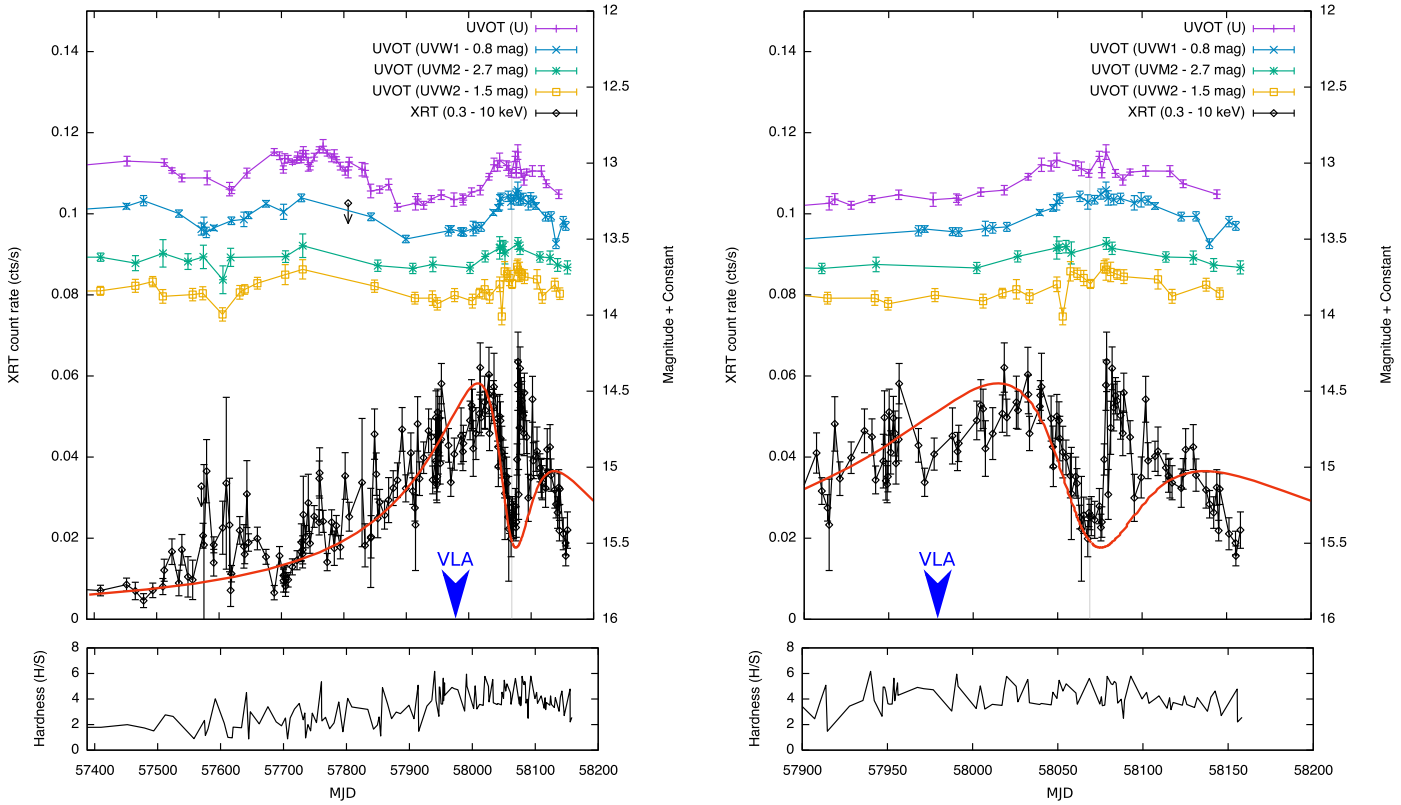

Figure 2. Left panel: the 0.3–10.0 keV and the Ultraviolet and Optical Telescope (UVOT) light curves of J2032 (from 2016 to 2018 January; 95% upper limits for non-detection epochs) with the hardness ratio evolution (H/S, where $S = 0.3$–1.5 keV and $H = 1.5$–10 keV) in the lower panel. Right panel: the zoom-in version for the periastron passage. Vega magnitude system is used for the UVOT light curve. For the hardness ratio plots, only those data points with uncertainties less than 2 are shown. The periastron date and the VLA observing date (2017 August 14 or MJD 57979) were indicated by a gray vertical line and a blue arrow, respectively. Finally, the red solid line shows the model light curve with $\alpha = 2$ for the radial distribution of the magnetization, and 40% of the speed of the post-shocked flow assumed in Takata et al. (2017). A more detailed description for the model can be found in Takata et al. (2017).

(Takata et al. 2017). In the model, the X-rays are dominated by the synchrotron emission from the post-shocked pulsar wind with the shock geometry calculated based on $\eta \sim 0.02$, which is the momentum ratio of the spin-down power of the pulsar ($L_{\rm sd} \sim 1.7 \times 10^{35}\,{\rm erg\,s^{-1}}$) to the stellar wind. The Doppler boosting effect due to the finite velocity of the shocked pulsar wind were also considered, assuming a constant bulk velocity of the post-shock pulsar along the shock-cone that was calculated based on the jump condition of a perpendicular magnetohydrodynamics (MHD) shock (Kennel & Coroniti 1984).

By comparing the model to the XRT light curve before 2017, the rapid X-ray flux increase in 2013–2016 implies a radial evolution with an index of $\alpha = 2$–3 (Takata et al. 2017). In addition, a rapid decrease in X-rays around the periastron was predicted, based on (i) an increase of the magnetization parameter at the shock (i.e., $\sigma > 1$), and (ii) the suppression due to the Doppler boosting effect. The Doppler boosting effect would also make the observed X-ray modulation asymmetric about the periastron date as the viewing angle changes. These features have all been seen in the observed *Swift*/XRT light curve shown in Figure 2, although the post-periastron X-ray emission predicted in Takata et al. (2017) was slightly underestimated (see Figure 16 with $\alpha = 2$ in the reference). This likely implies an overestimation of the speed of the post-shocked pulsar wind flow, and hence the X-ray flux suppression due to the Doppler boosting effect. We therefore reduced the assumed speed of the post-shock flow down to 40%, and the resultant model light curve matches the general trend of the XRT light curve reasonably well (Figure 2).

Understanding the flare-like X-ray structure observed around MJD 58080–58100 in the pulsar wind/stellar wind interaction model is not straightforward. Alternatively, this X-ray enhancement could be caused by the pulsar and Be stellar disk interaction, which abruptly changes the shock structure. The radius of the shock (from the pulsar) induced by the interaction can be determined by

$$r_s = \left(\frac{L_{\rm sd}}{2\pi\rho_d v_r^2 c}\right)^{1/2}, \quad (3)$$

where ρ_d is the disk-mass density at the pulsar's position and v_r is the relative velocity between the pulsar and the disk rotation. If the scale height of the Be stellar disk at the pulsar's position is larger than the shock radius, the disk can confine most of the pulsar wind, which could lead to an X-ray flux enhancement as suggested in Takata et al. (2012). In Takata et al. (2017), we discussed that if the base density of the Be stellar disk is larger than $\rho_0 > 10^{-10}\,{\rm g\,cm^{-3}}$ and the pulsar/Be stellar disk interaction occurs at the periastron passage, the Be stellar disk can make a cavity of the pulsar wind around the pulsar, and enhance the X-ray emission. The flare-like X-ray enhancement lasted for about 20 days, which is a much longer period compared to the timescale needed for the pulsar to cross the Be stellar disk (i.e., $t_c \sim H/v_p \sim 2$ days, where $H \sim 0.1$ au is the scale height of the Be stellar disk at the pulsar orbit and $v_p \sim 10^7\,{\rm cm\,s^{-1}}$ is the pulsar's orbital velocity). However,

some disk matter could pile up in front of the pulsar when it is passing through the disk. This phenomenon has been shown possible in the 3D smoothed particle hydrodynamic simulation by Takata et al. (2012). This piled-up disk matter will influence the shock structure, and hence the X-ray emission, until it is dispersed by the pressure of the nearby gas. The timescale of the dispersion can be estimated as $t_d \sim H/c_s \sim 20$ days, where $c_s \sim 10$ km s^{-1} is the sound speed of the Be stellar disk (Okazaki et al. 2011), and it is well consistent with the timescale of the X-ray flare.

5.2. Possible Orbital Modulation in UV

In the UVOT light curve, there is a clear UV brightening on a timescale of about 100 days right at the periastron passage. Unfortunately, the UV brightening is strongly contaminated by MT91 213 (see the strong intrinsic variability of the Be star before MJD 57900 in Figure 2), and therefore not much information can be extracted. In fact, it is entirely possible that the UV brightening is totally unrelated to the periastron passage, but merely a time coincidence to the intrinsic brightness change of the Be star.

In Takata et al. (2017), we discussed the possibility that if the density of the Be stellar disk is sufficiently high, some matter of the disk could be captured by the pulsar during the periastron passage and a short-lived (e.g., weeks) UV-emitting accretion disk can be formed around the pulsar. However, the accretion disk would be very faint compared to the Be star/disk (a factor of $\gg$10 lower), and therefore the UV band (below 0.01 keV) will still be completely dominated by the emission from the Be star/disk (see Figure 22 in Takata et al. 2012). Obviously, the faint UV emission from the aforementioned accretion disk is not comparable to the UV brightening, which has a relatively high amplitude of $\sim$0.2 mag (about 20% of the Be star/disk). We therefore conclude that the enhanced UV emission is unlikely from the accretion disk.

5.3. Gamma-ray Light Curve

We did not see any significant GeV modulation in the *Fermi*-LAT light curve, which is not totally unexpected given the strong contamination from the bright pulsed γ-ray emission of PSR J2032+4127, as we have mentioned. Performing pulsar gating could remove the unwanted pulsar's contribution, and hence recover the GeV modulation due to the pulsar/stellar winds interactions, if an accurate ephemeris of the pulsar during the periastron passage is provided by radio timing observations.

Yet, there was a very marginal γ-ray flux drop (about 50% of the mean flux) observed right after the periastron passage (the middle panel of Figure 1). While the drop is totally consistent with the statistical fluctuations seen in other epochs of the light curve, indicating that the drop is insignificant, we note that a possible accretion flow discussed in Section 5.2 can indeed shut down the γ-ray emission from the pulsar's magnetosphere (see, e.g., Takata et al. 2017), resulting in a similar light curve feature. In this scenario, the radio pulsation should have been shut down. Radio observations taken in the post-periastron epoch would be very useful to test the idea.

Support for this work was partially provided by the National Aeronautics and Space Administration through *Chandra* Award Number GO7-18036X issued by the *Chandra* X-ray Observatory Center, which is operated by the Smithsonian Astrophysical Observatory for and on behalf of the National Aeronautics Space Administration under contract NAS8-03060. J.T. is supported by NSFC grants of Chinese Government under 11573010 and U1631103. P.H.T. is supported by the NSFC grant 11633007. Both are supported by NSFC grant 11661161010. A.K.H.K. is supported by the Ministry of Science and Technology of the Republic of China (Taiwan) through grants 105-2119-M-007-028-MY3 and 105-2112-M-007-033-MY2. C.Y.H. is supported by the National Research Foundation of Korea through grant 2016R1A5A1013277. K.S.C. is supported by GRF grant under 17302315. We acknowledge the use of public data from the *Swift* data archive. We also acknowledge the use of data and software facilities from the FSSC, managed by the HEASARC at the Goddard Space Flight Center. The National Radio Astronomy Observatory is a facility of the National Science Foundation operated under cooperative agreement by Associated Universities, Inc.

Facilities: Swift, *Fermi*, VLA.

ORCID iDs

K. L. Li https://orcid.org/0000-0002-0439-7047
J. Takata https://orcid.org/0000-0002-8731-0129
P. H. T. Tam https://orcid.org/0000-0002-1262-7375
C. Y. Hui https://orcid.org/0000-0003-1753-1660

References

Abdo, A. A., Ackermann, M., Ajello, M., et al. 2009, Sci, 325, 840
Acero, F., Ackermann, M., Ajello, M., et al. 2015, ApJS, 218, 23
Bodaghee, A., Tomsick, J. A., Pottschmidt, K., et al. 2013, ApJ, 775, 98
Camilo, F., Ray, P. S., Ransom, S. M., et al. 2009, ApJ, 705, 1
Chernyakova, M., Neronov, A., van Soelen, B., et al. 2015, MNRAS, 454, 1358
Coe, M. J., Steele, I. A., Ho, W. C. G., et al. 2017, ATel, 10920, 1
Coroniti, F. V. 1990, ApJ, 349, 538
Dubus, G. 2013, A&ARv, 21, 64
Evans, P. A., Beardmore, A. P., Page, K. L., et al. 2007, A&A, 469, 379
Evans, P. A., Beardmore, A. P., Page, K. L., et al. 2009, MNRAS, 397, 1177
Ho, W. C. G., Ng, C.-Y., Lyne, A. G., et al. 2017, MNRAS, 464, 1211
Kennel, C. F., & Coroniti, F. V. 1984, ApJ, 283, 694
Kirk, J. G., & Giacinti, G. 2017, PhRvL, 119, 211101
Kirk, J. G., & Mochol, I. 2011, ApJ, 729, 104
Li, K. L., Kong, A. K. H., Tam, P. H. T., et al. 2017, ApJ, 843, 85
Lyne, A. G., Stappers, B. W., Keith, M. J., et al. 2015, MNRAS, 451, 581
Lyubarsky, Y., & Kirk, J. G. 2001, ApJ, 547, 437
Massey, P., & Thompson, A. B. 1991, AJ, 101, 1408
Mirzoyan, R., & Mukherjee, R. 2017, ATel, 10971, 1
Okazaki, A. T., Nagataki, S., Naito, T., et al. 2011, PASJ, 63, 893
Petropoulou, M., Vasilopoulos, G., Christie, I. M., Giannios, D., & Coe, M. J. 2018, MNRAS, 474, L22
Ray, P. S., Kerr, M., Parent, D., et al. 2011, ApJS, 194, 17
Reed, B. C. 2003, AJ, 125, 2531
Takata, J., Okazaki, A. T., Nagataki, S., et al. 2012, ApJ, 750, 70
Takata, J., Tam, P. H. T., Ng, C. W., et al. 2017, ApJ, 836, 241
Tam, P. H. T., Li, K. L., Takata, J., et al. 2015, ApJL, 798, L26
Veritas & MAGIC Collaborations 2017, ATel, 10810, 1